



## Galvanic Deposition of Nanoporous Si onto 6061 Al Alloy from Aqueous HF

Aarti Krishnamurthy,<sup>a</sup> Don H. Rasmussen,<sup>b,c</sup> and Ian I. Suni<sup>b,c,\*</sup>

<sup>a</sup>Department of Chemistry and Biomolecular Science, <sup>b</sup>Department of Chemical and Biomolecular Engineering, and <sup>c</sup>Materials Science and Engineering PhD Program, Clarkson University, Potsdam, New York 13699-5705, USA

We report galvanic deposition of Si onto 6061 Al alloy from dilute aqueous hydrofluoric acid (HF) at pH 2.5. The overall reaction involves reduction of  $\text{SiF}_6^{2-}$  to Si with simultaneous oxidation and dissolution of Al. The Si film is about 12  $\mu\text{m}$  thick after 6 h of deposition. High resolution scanning electron microscopy shows that these Si films are nanoporous, with pore sizes ranging from 3 to 8 nm. The nanoporous Si films oxidize rapidly upon sample emersion. Elemental analysis by energy dispersive X-ray spectroscopy demonstrates that the as-deposited film contains 1–3 atom % Al, 3–6 atom % Cu, and 90–95 atom % Si. We believe that this is the first report of electrochemical deposition of Si thin films that does not involve organic solvents or molten salt electrolytes.

© 2010 The Electrochemical Society. [DOI: 10.1149/1.3521290] All rights reserved.

Manuscript submitted August 3, 2010; revised manuscript received November 4, 2010. Published December 3, 2010.

While the market for photovoltaic cells is currently dominated by thick film Si solar cells, thin film crystalline, polycrystalline, and amorphous Si solar cells have also been intensively investigated.<sup>1</sup> Optical absorption in Si solar cells occurs mainly within the top micrometer of Si, so the rest of the Si wafer in thick film solar cells merely provides mechanical support. While thick film Si solar cells can directly employ Si wafer technology and materials from integrated circuit manufacturing, thin film Si solar cells provide obvious long-term cost advantages. In addition to photovoltaic applications, Si thin films are of interest for silicon-on-sapphire complementary metal oxide semiconductor technology,<sup>2</sup> for anode materials in Li ion batteries,<sup>3,4</sup> and for corrosion-resistant coatings.<sup>5</sup>

Si thin films are typically deposited by expensive vacuum methods such as chemical vapor deposition and plasma-enhanced chemical vapor deposition.<sup>1</sup> In addition, Si thin films are typically deposited from silane, which is both highly pyrophoric and moisture sensitive. Electrochemical methods for depositing thin film solar cell materials are highly advantageous due to their low cost, scalability to large surface areas, and manufacturability.<sup>6</sup> However, Si is a highly active metal, so the standard reduction potential of  $\text{SiO}_2$  [−0.90 V vs normal hydrogen electrode (NHE)] is more cathodic than the standard reduction potential of water (−0.83 V vs NHE),<sup>7</sup> making electrochemical deposition of Si from aqueous electrolytes notoriously difficult.

Si electrodeposition from molten salts at elevated temperatures ( $\geq 750^\circ\text{C}$ ) has a long history.<sup>8–11</sup> However, Si electrodeposition at room temperature has only relatively recently been achieved from organic solvents<sup>12–17</sup> and from room temperature ionic liquids.<sup>18–23</sup> Here we report galvanic deposition of nanoporous Si onto Al from solutions of dilute aqueous hydrofluoric acid (HF) at pH 2.5, with 12  $\mu\text{m}$  thick Si films grown after 6 h. Energy dispersive X-ray spectroscopy (EDX) measurements show that the as-deposited film contains mainly Si, Cu, and Al.

### Experimental

Semiconductor grade 10 wt % HF and concentrated  $\text{HNO}_3$  were obtained from J. T. Baker,  $\text{Na}_2\text{SiF}_6$  was obtained from Sigma-Aldrich, and 6061 Al alloy was obtained from McMaster Carr. For Al electrochemistry, all measurements were performed using a three-electrode setup with a 12 mm diameter 6061 Al alloy working electrode rotated at 850 rpm with a rotating disc electrode, Pt spiral counter electrode, and a reference SCE. A 6061 Al alloy typically contains 0.8–1.2 wt % Mg, 0.4–0.8 wt % Si,  $\leq 0.70$  wt % Mg, 0.15–0.40 wt % Cu, 0.04–0.35 wt % Cr, and smaller amounts of

Mn, Ti, and Zn. For some of the galvanic deposition experiments, 99.99% pure Al was purchased from ESPI Metals. For Si electrochemistry, B-doped ( $2 \times 10^{19} \text{ cm}^{-3}$ ) degenerate Si(100) wafers with a resistivity of 0.001–0.005  $\Omega \text{ cm}$  were purchased from University Wafer. The electrical connection to the Si wafer's back side was made using a Ga–In eutectic.

Voltammetry experiments were controlled with an EG&G PAR model 273A potentiostat/galvanostat. Impedance measurements were made by coupling this potentiostat with a Solartron 1250B frequency response analyzer over the frequency range 0.01 Hz–10 kHz, using an ac probe voltage of 8 mV. The Si film thickness was measured with a JEOL model 7400F field emission scanning electron microscope at both 45 and 90°.

### Results and Discussion

Figure 1 illustrates a voltammogram of the Al working electrode rotated at 850 rpm in 10 mM HF + 1 mM  $\text{HNO}_3$  (pH 2.5). An addition of 20 mM  $\text{Na}_2\text{SiF}_6$  to this electrolyte had no discernable effect on the voltammetry results. Figure 1 illustrates that this electrolyte is quite corrosive to Al, with anodic currents from Al oxidation and dissolution observed at all potentials anodic to −1000 mV vs SCE. This is the reason why such a high scan rate (50 mV/s) was employed. Immersion of the Al working electrode rotated at 850 rpm without potential control into 10 mM HF, 1 mM  $\text{HNO}_3$ , and 20 mM  $\text{Na}_2\text{SiF}_6$  for 6 h results in the growth of a Si film about 12  $\mu\text{m}$  thick. The open circuit potential was measured during Si deposition and varied between −700 and −900 mV vs SCE, as shown in Fig. 2. The as-grown film is dark gray in solution but changes color to light gray after exposure to laboratory air for 1 h and then to white upon overnight exposure.

Figures 3 and 4 present scanning electron microscopy (SEM) images following growth of a 12  $\mu\text{m}$  Si film as described above. Figure 3 illustrates the 12  $\mu\text{m}$  Si film (middle) atop the Al substrate (bottom) and appears to show a compact Si deposit. However, the higher resolution image in Fig. 4 shows that the Si deposit contains nanoscale porosity, with pore sizes ranging from 3 to 8 nm. Other methods that have been reported for room temperature Si electrodeposition similarly yield porous Si films, as discussed elsewhere.<sup>15</sup> X-ray diffraction studies of our galvanic Si films, both immediately after deposition and after overnight ambient exposure, show no diffraction peaks, indicating that our deposits are amorphous.

The Si deposit is grown atop Al by galvanic deposition, otherwise known as immersion plating, where a more noble metal is reduced and deposited onto a less noble substrate that is simultaneously oxidized and dissolved. The cathodic (1), anodic (2), and overall (3) reactions for galvanic deposition of Si onto Al are<sup>7</sup>

\* Electrochemical Society Active Member.

<sup>z</sup> E-mail: isuni@clarkson.edu

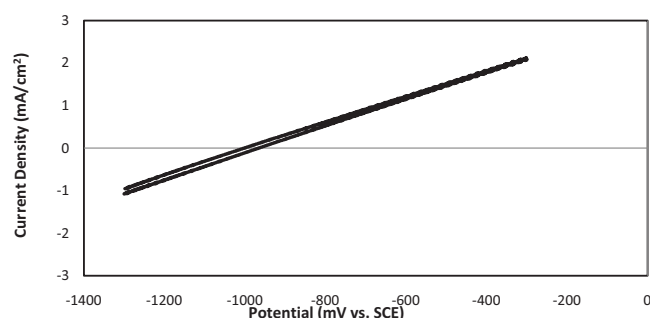


**Figure 1.** Voltammetry of the 6061 Al electrode rotated at 850 rpm in 10 mM HF + 1 mM HNO<sub>3</sub> at a scan rate of 50 mV/s.

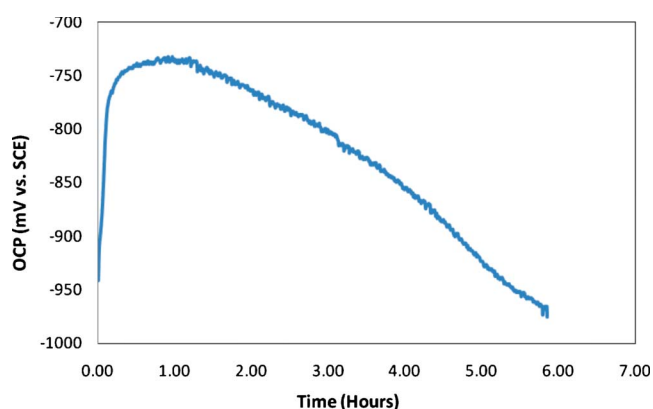


**Figure 2.** (Color online) Open circuit potential measured as a function of time at the Al electrode during Si deposition from 10 mM HF, 1 mM HNO<sub>3</sub>, and 20 mM Na<sub>2</sub>SiF<sub>6</sub>.

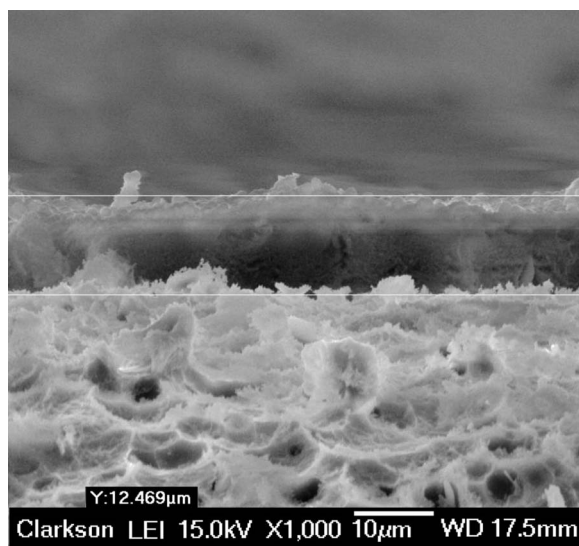


**Figure 3.** SEM image at a 45° angle after 6 h of Si deposition from 10 mM HF, 1 mM HNO<sub>3</sub>, and 20 mM Na<sub>2</sub>SiF<sub>6</sub>. The Al substrate is at the bottom and the Si film is in the middle.

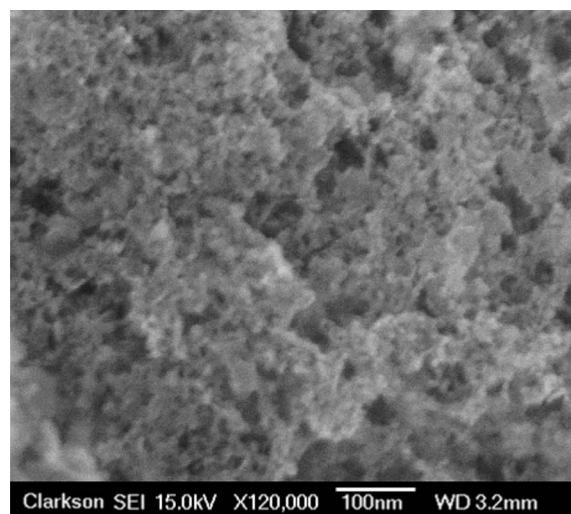
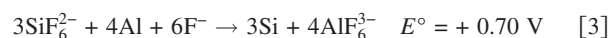
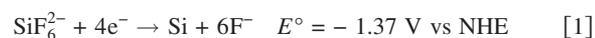


**Figure 4.** SEM image of Si deposit at 1,20,000 × magnification, illustrating nanoscale porosity.



Reaction 2 is written as an oxidation reaction, so the potential given is the opposite of the standard reduction potential. The standard potential given for the overall reaction 3 is positive, indicating a spontaneous reaction. Although reactions 1-3 are most obvious, one cannot rule out the possibility of intermediate oxidation states of Si and Al being involved. Reactions similar to those above have been widely reported for galvanic deposition of a variety of metals onto Si from aqueous HF solutions, as recently reviewed.<sup>24,25</sup> Such processes were originally studied to understand contamination of Si wafers during wet cleaning with HF but have also been proposed for a variety of technologies involving fabrication of metal nanostructures and thin films.<sup>24,25</sup>

However, such methods are not limited to Si substrates, because our laboratory has reported galvanic deposition of Cu onto Ta from aqueous HF.<sup>26</sup> The present research extends such methods to Al substrates and to deposition of Si films. The current method for galvanic deposition of Si may be limited to a few highly active metal substrates, such as Al, that are anodic to Si in HF.<sup>7</sup> Fortunately, Al is the substrate onto which amorphous Si is typically deposited within thin film solar cells.<sup>1</sup> The current process is also quite similar to the double zincate process for galvanic deposition of Zn onto Al, as will be described in more detail below.

The EDX spectrum in Fig. 5 illustrates that the deposit contains Si, Al, Cu, and O. The significant O peak in the EDX spectrum is believed to arise from sample transfer through air, as has been previously observed by other research groups.<sup>15</sup> Counting only the heavy elements, EDX analyses of several Si deposits yield the following range of compositions: 1–3 atom % Al, 3–6 atom % Cu, and 90–95 atom % Si. Thus, the Si films contain significant Al, which probably cannot be avoided, because Al oxidation, dissolution, and transport through the growing Si film is part of the galvanic Si deposition process described above.

The Si films also contain significant Cu, which probably arises from the 6061 Al alloy itself, not from the solution phase, for the following reasons. First, galvanic Si deposition onto 99.99% pure Al results in a Si deposit that is removed by convective forces associated with electrode rotation at 850 rpm, resulting in Si flakes at the bottom of the cell. EDX analysis of these Si flakes does not show significant Cu incorporation. Second, atomic absorption spectro-

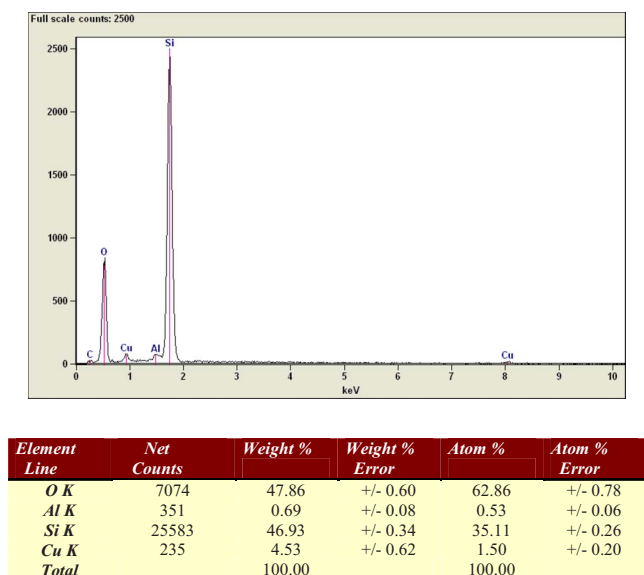


**Figure 5.** (Color online) EDX results after 6 h of Si deposition from 10 mM HF, 1 mM HNO<sub>3</sub>, and 20 mM Na<sub>2</sub>SiF<sub>6</sub>.

copy shows that the galvanic deposition bath contains only 140 ppb Cu, which is likely too low to yield the observed levels of Cu incorporation. It is possible that some of Si in the galvanic deposit arises from the 6061 Al alloy substrate as well.

Si adhesion was not quantitatively studied. Si film adhesion was good enough to survive convection associated with 850 rpm electrode rotation, but the Si film could be scratched off following sample emersion. However, the film adhesion was greatly improved after sample drying. As mentioned above, galvanic Si deposition from identical solutions onto 99.99% pure Al yielded poorly adherent deposits, so obtaining adequate adhesion depends on the presence of other elements in the 6061 Al alloy. Cu in this alloy is noble to both Al and Si, so Cu should either not dissolve or immediately redeposit in the galvanic deposition bath. We suggest that the Si film is anchored to Cu atoms within the 6061 Al alloy as Al dissolves from within the alloy.

The mechanism of galvanic Si deposition may be similar to that of galvanic Zn deposition onto Al, which is widely used for double zincate treatment of Al alloys to prepare the surface for subsequent electrodeposition or electroless deposition.<sup>27-30</sup> Cu pretreatment has been employed to improve Zn nucleation during the double zincate process<sup>30</sup> and increased Cu concentration at the Al–metal interface has been reported.<sup>28</sup> In addition, variations in the effectiveness of double zincate treatment with Al alloy content have been reported.<sup>30</sup>

As mentioned above, we expect that the Si surface deposited in 10 mM HF + 1 mM HNO<sub>3</sub> (pH 2.5) is not oxidized in situ, but is instead oxidized during sample emersion. Si oxidation in situ would cause reactions 1–3 to cease, because the surface would be coated with an electrical insulator. In addition, the color change observed upon sample emersion is consistent with gradual Si oxidation. One might expect possible Si oxidation in 10 mM HF + 1 mM HNO<sub>3</sub> (pH 2.5) to be well-understood, but this is not the case, because the Si film is deposited under conditions quite different from those employed for HF cleaning of Si. Here we report growth of a heavily Al-doped Si film from solutions with low F<sup>−</sup> concentrations (10 mM) at quite cathodic potentials (−700 to −900 mV vs SCE). By comparison, HF cleaning of Si wafers involves much higher F<sup>−</sup> concentrations (100 mM to 5.0 M) of moderately doped n- or p-type Si. In addition, Si electrochemistry in HF has been studied primarily at much more anodic potentials, where Si dissolution occurs with porous Si formation or with electropolishing.<sup>31</sup>

Using infrared spectroscopy for direct observation of the Si–H

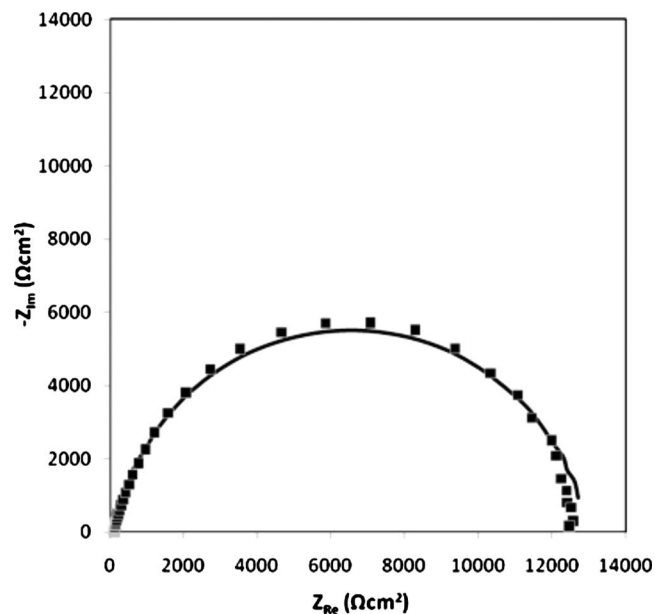


**Figure 6.** Nyquist plot illustrating the impedance results for degenerate Si at −800 mV vs SCE in 10 mM HF + 1 mM HNO<sub>3</sub>.

and Si–O vibrational modes, Chazalviel and co-workers have closely studied the transition between H- and O-terminated surfaces as a function of HF concentration and applied potential.<sup>32-34</sup> Even in dilute HF solutions, they observe a transition from H- to O-terminated Si at potentials considerably anodic to those observed here.<sup>32-34</sup> This supports our hypothesis that Si is not oxidized in the solutions studied here. The observations of Chazalviel and co-workers, and those of other researchers, have been incorporated into models of Si etching in HF solutions, where the balance between H- and O-terminated Si surface coverage is believed to depend on a complex balance between kinetic and thermodynamic factors.<sup>31</sup> Even at more anodic potentials where Si etching begins, the reactivity of the surface is determined by the number of O-terminated sites, but the fractional surface coverage of these highly reactive sites is believed to remain small, with the bulk of the surface still H-terminated.<sup>31</sup>

Insight into the nature of the Si–electrolyte surface can also be obtained from electrochemical studies of highly doped Si, where no space charge layer forms at either Si interface (electrolyte or back side electrical contact). Voltammetry studies of degenerate Si in 10 mM HF + 1 mM HNO<sub>3</sub> (not shown) do not reveal any cathodic or anodic features, so impedance studies of degenerate Si probe only the nature of the electrochemical interface. Figure 6 presents a Nyquist plot of the results from electrochemical impedance spectroscopy (EIS) for degenerate Si in 10 mM HF + 1 mM HNO<sub>3</sub> at −800 mV vs SCE. These data were fit to a Randles equivalent circuit, with the differential capacitance replaced by a constant phase element, yielding the best-fit equivalent circuit parameters shown in Table I.

These results can be compared to the detailed impedance study of Searson and Zhang of Si in HF at conditions close to those re-

**Table I.** Best-fit equivalent circuit parameters for impedance studies of degenerate Si at −800 mV vs SCE in 10 mM HF + 1 mM HNO<sub>3</sub>.

| Potential (mV vs SCE) | $R_s$ ( $\Omega \text{ cm}^2$ ) | $T_d \times 10^6$ ( $\mu\text{F cm}^{-2} \text{ s}^{n-1}$ ) | $n_d$     | $R_{ct}$ ( $\Omega \text{ cm}^2$ ) |
|-----------------------|---------------------------------|---|-----------|------------------------------------|
| −800                  | 147 (3)                         | 3.40 (10)   | 0.944 (5) | $7.51(21) \times 10^4$             |

ported here.<sup>35</sup> They distinguish between different surface conditions partly by the magnitude of the measured capacitance, which is expected to be in the nF cm<sup>2</sup>, μF cm<sup>-2</sup>, and mF cm<sup>-2</sup> range for a space charge layer, Helmholtz layer, and oxide layer, respectively.<sup>35,36</sup> Thus, a best-fit capacitance value in the μF cm<sup>-2</sup> range is considered as evidence of a Helmholtz layer in potential regimes and at dopant conditions where the surface is not oxidized and no space charge layer forms. The results in Table I are consistent with this criterion, supporting our assertion that Si oxide does not form in the solutions studied here.

In addition, Searson and Zhang observe that the charge transfer resistance ( $R_{ct}$ ) increases from 10<sup>1</sup> to 10<sup>3</sup> Ω cm<sup>2</sup> at potentials where Si dissolution occurs from 10<sup>4</sup> to 10<sup>5</sup> Ω cm<sup>2</sup> at more cathodic potentials, such as those studied here, where the surface is likely H-terminated.<sup>35</sup> The charge transfer resistance observed here (7.51 × 10<sup>4</sup> Ω cm<sup>2</sup>) is consistent with the results of Searson and Zhang. These results are consistent with the general observation that H-terminated Si is much more stable and unreactive than O-terminated Si, yielding somewhat higher  $R_{ct}$  at more cathodic potentials.<sup>31,35</sup>

The galvanic Si thin films deposited here can be compared with Si thin films electrodeposited at room temperature from organic solvents<sup>12-17</sup> and room temperature from ionic liquids (RTILs).<sup>18-23</sup> This is complicated by the wide variation in reported results between different research groups, which makes comparisons difficult. However, it has been suggested that compact Si film electrodeposition from organic solvents is limited to deposits ≤250 nm thick.<sup>20</sup> In addition, it has been suggested that Si films electrodeposited from organic solvents are always porous and oxidize rapidly upon ambient exposure.<sup>15</sup> Si thin films electrodeposited from RTILs onto flat substrates appear to have been limited to date to a thickness of several hundred nanometers. Regardless of the veracity of these generalizations, thick and compact Si films have not been grown to date by room temperature electrodeposition. In addition, many of the reported Si films are contaminated by impurity elements originating from the solvent. The galvanic Si films reported here suffer from many of these same issues. The primary advantages of the current method include its simplicity, the modest cost and toxicity of the reagents employed, and the ability to grow thick 12 μm Si films.

### Conclusions

Galvanic deposition of Si onto 6061 Al alloy occurs from solutions containing 10 mM HF, 1 mM HNO<sub>3</sub>, and 20 mM Na<sub>2</sub>SiF<sub>6</sub>. Si films about 12 μm thick are formed after 6 h of deposition. High resolution SEM indicates that the Si films are nanoporous, with pore sizes ranging from 3 to 8 nm. For this reason, the Si film appears to oxidize rapidly upon sample emersion. However, in situ measurements by EIS on degenerate Si yield capacitance and charger transfer resistance ( $R_{ct}$ ) values consistent with an H-terminated Si surface rather than an oxidized surface. This is consistent with previously reported studies of Si in dilute HF by infrared spectroscopy, confirming that Si is not oxidized in situ. Elemental analysis by EDX demonstrate that the as-deposited film contains 1–3 atom % Al, 3–6 atom % Cu, and 90–95 atom % Si.

### Acknowledgments

This research was supported by U.S. Army grant no. W911NF-05-1-0339 and the Center for Advanced Materials Processing (CAMP) at Clarkson University.

Clarkson University assisted in meeting the publication costs of this article.

### References

1. *Clean Electricity from Photovoltaics*, M. D. Archer and R. Hill, Editors, Imperial College Press, London (2001).
2. R. A. Johnson, P. R. de la Houssaye, C. E. Chang, P. F. Chen, M. E. Wood, G. A. Garcia, I. Lagnado, and P. M. Asbeck, *IEEE Trans. Electron Devices*, **45**, 1047 (1998).
3. L. B. Chen, K. Wang, X. H. Xie, and J. Y. Xie, *Electrochem. Solid-State Lett.*, **9**, A512 (2006).
4. T. L. Kulova, A. M. Skundin, Y. V. Pleskov, E. I. Terukov, and O. I. Kon'kov, *J. Electroanal. Chem.*, **600**, 217 (2007).
5. S. Guruvenket, M. Azzi, D. Li, J. A. Szpunar, L. Martinu, and J. E. Klemberg-Sapieha, *Surf. Coat. Technol.*, **204**, 3358 (2010).
6. I. M. Dharmadasaz and J. Haigh, *J. Electrochem. Soc.*, **153**, G47 (2006).
7. *Standard Potentials in Aqueous Solution*, A. J. Bard, R. Parsons, and J. Jordan, Editors, Marcel Dekker, New York (1985).
8. G. M. Rao, D. Elwell, and R. S. Feigelson, *J. Electrochem. Soc.*, **127**, 1940 (1980).
9. R. C. de Matthei, D. Elwell, and R. S. Feigelson, *J. Electrochem. Soc.*, **128**, 1712 (1981).
10. R. Boen and J. Bouteillon, *J. Appl. Electrochem.*, **13**, 277 (1983).
11. K. L. Carleton, J. M. Olson, A. Kibbler, and R. S. Feigelson, *J. Electrochem. Soc.*, **130**, 782 (1983).
12. A. K. Agrawal and A. E. Austin, *J. Electrochem. Soc.*, **128**, 2292 (1981).
13. C. H. Lee and F. A. Kroger, *J. Electrochem. Soc.*, **129**, 936 (1982).
14. P. R. Sarma, T. R. R. Mohan, S. Venkatachalam, J. Singh, and V. P. Sundesingh, *Mater. Sci. Eng., B*, **15**, 237 (1992).
15. J. P. Nicholson, *J. Electrochem. Soc.*, **152**, C795 (2005).
16. Y. Nishimura and Y. Fukunaka, *Electrochim. Acta*, **53**, 111 (2007).
17. T. Munisamy and A. J. Bard, *Electrochim. Acta*, **55**, 3797 (2010).
18. S. Z. el Abedin, N. Borissenko, and F. Endres, *Electrochem. Commun.*, **6**, 510 (2004).
19. N. Borissenko, S. Z. el Abedin, and F. Endres, *J. Phys. Chem. B*, **110**, 6250 (2006).
20. S. Z. el Abedin and F. Endres, *Acc. Chem. Res.*, **40**, 1106 (2007).
21. R. Al-Salman, S. Z. el Abedin, and F. Endres, *Phys. Chem. Chem. Phys.*, **10**, 4650 (2008).
22. J. Mallet, M. Molinari, F. Martineau, F. Delavole, P. Fricoteaux, and M. Troyon, *Nano Lett.*, **8**, 3468 (2008).
23. Y. Nishimura, Y. Fukunaka, T. Nishida, T. Nohira, and R. Hagiwara, *Electrochem. Solid-State Lett.*, **11**, D75 (2008).
24. S. Yae, N. Nasu, K. Matsumoto, T. Hagihara, N. Fukumuro, and H. Matsuda, *Electrochim. Acta*, **53**, 35 (2007).
25. C. Carraro, R. Maboudian, and L. Magagnin, *Surf. Sci. Rep.*, **62**, 499 (2007).
26. S. Sapra, H. Li, Z. Wang, and I. I. Suni, *J. Electrochem. Soc.*, **152**, B193 (2005).
27. D. S. Lashmore, *Plat. Surf. Finish.*, **72**, 36 (1985).
28. F. J. Monteiro and D. H. Ross, *Trans. Inst. Met. Finish.*, **62**, 155 (1985).
29. D. A. Hutt, C. Q. Liu, P. P. Conway, D. C. Whalley, and S. H. Mannan, *IEEE Trans. Compon. Packag. Technol.*, **25**, 87 (2002).
30. K. Azumi, S. Egoshi, S. Kawashima, and Y. Koyama, *J. Electrochem. Soc.*, **154**, D220 (2007).
31. K. W. Kolasinski, *Phys. Chem. Chem. Phys.*, **5**, 1270 (2003).
32. C. da Fonseca, F. Ozanam, and J. N. Chazalviel, *Surf. Sci.*, **365**, 1 (1996).
33. A. Belaidi, M. Safi, F. Ozanam, J. N. Chazalviel, and O. Gorochov, *J. Electrochem. Soc.*, **146**, 2659 (1999).
34. J. N. Chazalviel, A. Belaidi, M. Safi, F. Maroun, B. H. Erne, and F. Ozanam, *Electrochim. Acta*, **45**, 3205 (2000).
35. P. C. Searson and X. G. Zhang, *J. Electrochem. Soc.*, **137**, 2539 (1990).
36. J. C. Lin, C. M. Lai, W. D. Jehng, K. L. Huseh, and S. L. Lee, *J. Electrochem. Soc.*, **155**, D436 (2008).